DOI: 10.1002/chem.200903128

Exploring Group 14 Structures: 1D to 2D to 3D

Xiao-Dong Wen, Thomas J. Cahill, and Roald Hoffmann*[a]

Abstract: Various one-, two- and three-dimensional Group 14 (C, Si, Ge, Sn, and Pb) element structures at $P=$ 1 atm are studied in this work. As expected, coordination number (CN)—not an unambiguous concept for extended structures—plays an important part in the stability of structures. Carbon not only favors four-coordination, but also is quite happy with π-bonding, allowing three- and even two-coordination to compete. Highly coordinated ($CN>4$) discrete carbon molecules are rare; that "saturation of valence" is reflected in the instability of C extended structures with $CN>4$. Si and Ge are quite similar to each other in their preferences. They are less biased in their coordination than C, allowing (as their molecular structures do) $CN=5$ and 6, but tending towards four-coordination. Sn and Pb 3D structures are very flexible in their bonding, so that in these elements four- to twelve-coordinate structures are close in energy. This lack of discrimination among ordered structures also points to an approach to the liquid state, consistent with the low melting point of Sn and Pb. The Group 14 liquid structures we simulate in molecular dynamics calculations show the expected, effective, first coordination number increase from 5.1 for Si to 10.4 for Pb. A special point of interest emerging from our study is the instability of potential multilayer graphene structures down Group 14. Only for C will these be stable; for all the other Group 14 elements pristine, unprotected, bi- and multilayer graphenes should collapse, forming "vertical" bonds as short as the in-plane ones.

Keywords: coordination modes · density functional calculations · dimensionality · Group 14 elements · molecular dynamics

Introduction

A starting point, and questions: The role of dimensionality in the structure of any material is fascinating. The complexity that ensues from variation in dimensionality, and from structural alternatives, is rich in emergent properties even for elemental structures. Witness the splurge of activity in two-dimensional carbon, graphene.[1] The geometrics and energetics of one-, two-, and three-dimensional Group 14 elemental structures at $P=1$ atm is the subject of this paper.

But we came to investigate to this very general problem from a rather different starting point. In a fascinating group of compounds, the Au_2MP_2 ($M=$Hg, Tl, Pb) phases, Eschen and Jeitschko found sensibly one-dimensional, zero-valent Hg, Tl, or Pb chains.[2] We took these out of their inorganic matrix (theoretically), and studied them on their own.[3] To our initial surprise, the one-dimensional (1D) chains (we focus on Pb for the moment) did not want to remain linear, but instead kinked. Further deformations to spirals were found to be thermodynamically more favorable. Two-dimensional (2D) networks were at lower energy, and three-dimensional (3D) ones still lower, with interesting differences depending on crystal structure type.

We should not have been surprised. In a nutshell, solid Pb "wants" to be metallic, close-packed face-centered cubic (fcc) in structure, and thus 12-coordinate. The simplest 1D and 2D structures don't allow this and as a result their energy is higher. For Pb, within a dimensionality (imposed by a human being, the calculator), the more nearest neighbors (up to the optimum of 12) a geometry allows, the lower energy it will be. This explains the preference for tight helices over linear chains.

[a] Dr. X.-D. Wen, T. J. Cahill, Prof. R. Hoffmann
Department of Chemistry and Chemical Biology
Cornell University, Baker Laboratory, Ithaca
New York 14853-1301 (USA)
Fax: (+1) 607-255-4137
E-mail: rh34@cornell.edu

Supporting information for this article is available on the WWW under http://dx.doi.org/10.1002/chem.200903128. It contains details of all the structures that were optimized, with the corresponding bond lengths, DFT functional utilized, phonon dispersions of graphene and graphite, energetics of transformations, band structure and DOS of Group 14 graphene structures, simulated liquid Si, Ge, Sn, and Pb structures and corresponding computed radial distribution functions and fitting functions.

Let us now step back, pretty far back, from this specific starting point and consider the energetics of elemental structures as a function of dimensionality. Group 14, crossing as it does the metal–nonmetal boundary, is a good place to explore this problematic. The questions that arise, broadly phrased, include, "What are the relative energies of various stable and metastable structures in one, two, and three dimensions? Why do they come out the way they do? What are the magnitudes of the potential energy barriers (activation energies) separating the various minima? How do the minima and barriers vary across the periodic table? What is the relationship of the relative energy of the various structures to the solid to liquid transition in these materials?" These questions are made very much real for carbon by the synthesis and characterization of fullerenes, nanotubes, and graphene sheets, several classes of low-dimensional carbons. Will one find such structures for Si, Ge, Sn, and Pb? Will they be kinetically persistent?

We will offer some chemically mediated answers to these questions, supported by theoretical computations. All of the work reported here is at 1 atm. In later work we extend these considerations to covalently and ionically bonded binary compounds, and Group 14 elements at elevated pressure.

Structural choices: What structures to consider? The 3D geometries are the easiest to choose—they should include most typical crystal types and they should offer a range of coordination geometries. Clearly, C will want three or four nearest neighbors (graphite and diamond polytypes), at least at ambient pressure, while solid Pb, being the metal that it is, will seek out 12 nearest neighbors, fcc. Figure 1 shows the set of 3D structures we chose to investigate, in order of increasing coordination number (CN)—they include graphite (two polytypes; **1**, -ABAB- stacked, **2**, -AAAA- stacked), diamond (**3**), β-tin (**4**), simple cubic (**5**), simple hexagonal (**6**), body-centered cubic (bcc; **7**), face-centered cubic (fcc; **8**), and hexagonal close packing (hcp; **9**). Of course, there are other elemental structures; these nine should offer enough range in CN (3–12) for a trend for each element to emerge.

For reasons that will become clear, we arrange these structures in order of increasing CN, which is specified under to the structure number. The notion of coordination number is inherently ambiguous. Is graphitic structure **1** (-AAAA-) three or five-coordinate? That depends on the ratio of in-plane and out-of-plane distances, and our "cut-off" for defining a distance as bonding. We will return shortly to the problems hidden in the seemingly simple concept of coordination number. For the moment we term structure **1** as 3+2 coordinate, specifying the number of nearest and next-nearest neighbors; though, as we will see, next-nearest neighbors have a way of becoming nearest ones. The same uncertainty (what coordination number characterizes an atom in this structure?) rears its head for many structures.

For the 1D and 2D structures some highly symmetrical geometries are evident (just satisfying our aesthetic prejudice for simplicity), such as a linear chain, a square, and a honeycomb net. Beyond these, the choices are somewhat arbitrary. The 2D starting geometries shown in Figure 2 include the honeycomb net or graphene (**10**), two-layer graphenes (**11** and **12**), the square-planar sheet (**13**), kagome net (**14**), wavy or corrugated square sheet (**15**), "cubic" planar or double square sheet (**16**), rhombohedral planar or trigonal prism sheet (**17**), and a triangular sheet (**18**).

The 1D starting geometries shown in Figure 3 start simply enough with a linear chain (**19**), then branch out into wide angle zigzag (**20**), ladder (**21**), (3,3) single-walled nanotube (SWNT) (**22**), extended spirocycles (**23** and **24**), small angle zigzag (**25**), helical (**26** and **27**), hexagonal pipe (**28**), and cubic chain (**29**) geometries. Again, these are arranged in a rough order of increasing coordination number.

Actually, we modeled of the PAW-LDA (computational details DFT calculations we use are given in the section on Computational Methods) 42 possible structures for C, Si, Ge, Sn, and Pb, of which the 29 shown in Figures 1, 2 and 3

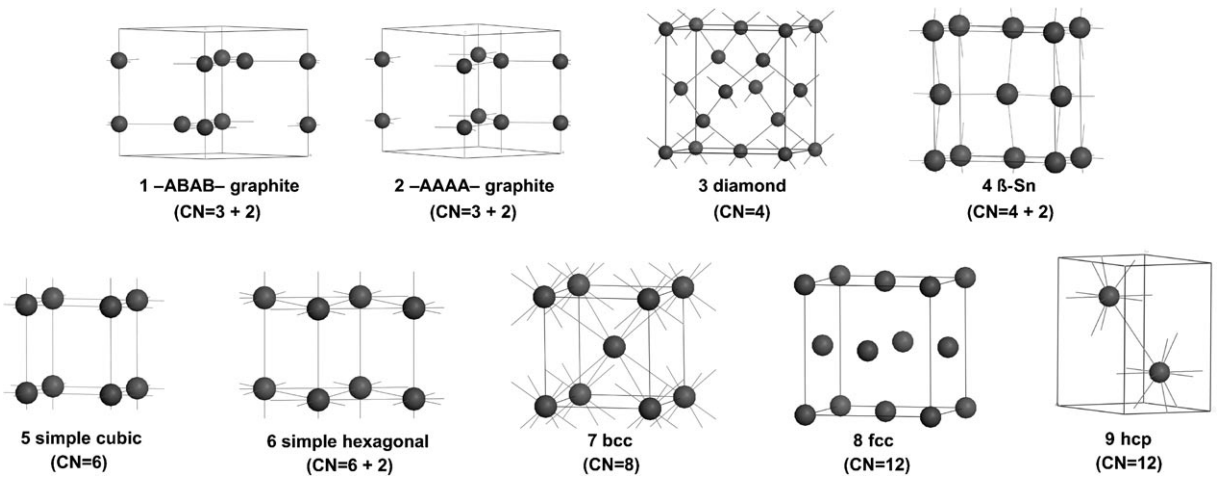

Figure 1. The nine different 3D starting geometries for C, Si, Ge, Sn and Pb.

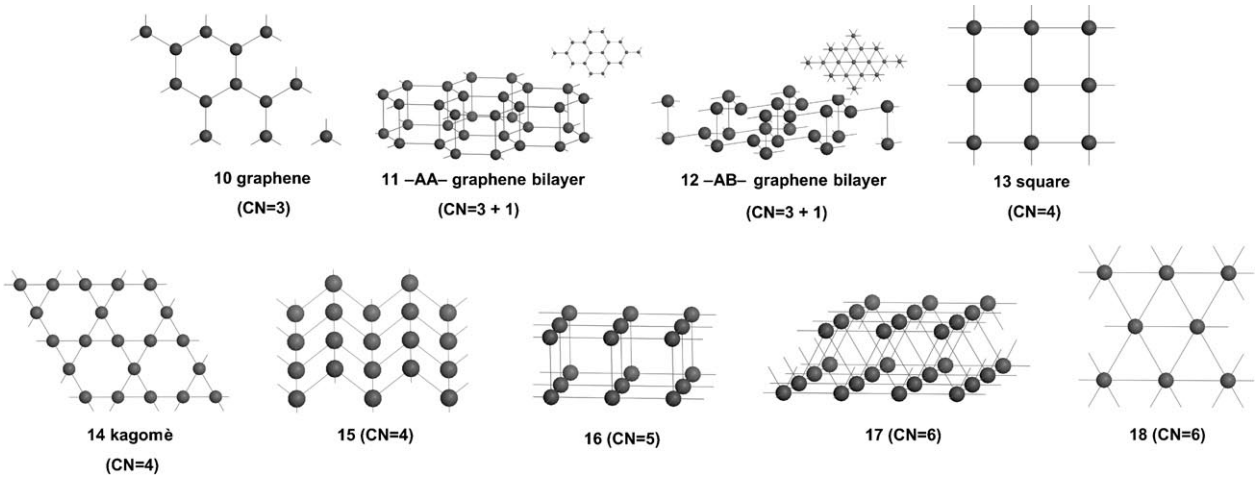

Figure 2. Different 2D starting geometries for Group 14 structures.

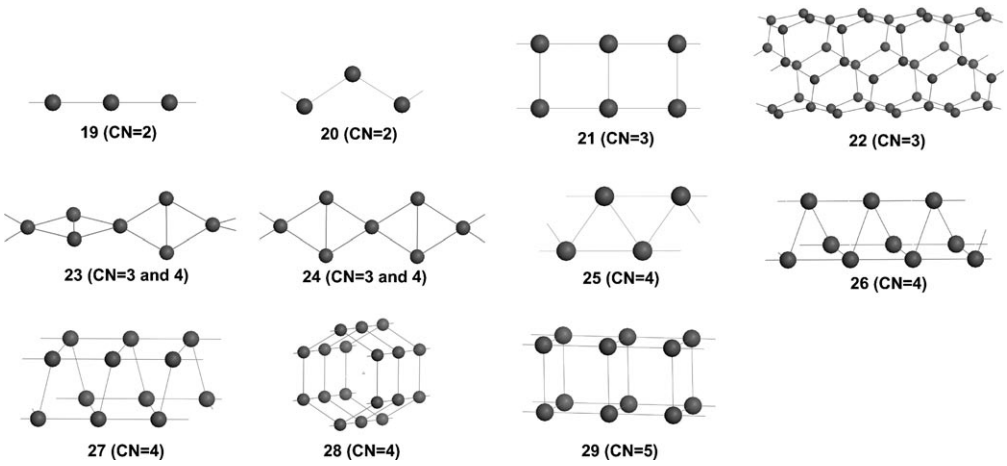

Figure 3. Eleven different 1D starting geometries for C, Si, Ge, Sn and Pb structures.

are a subset. All optimized structures, bond lengths, and energies can be found in the Supporting Information. All of the considerations in this paper are at ambient pressure. In a future paper, we will discuss how the elemental landscapes change at elevated pressure.

Coordination number (CN): One should not wait any longer to address explicitly the useful, but fuzzy, concept of coordination number. There is usually (but not always[4]) little ambiguity in a 0D object, such as a molecule—C in CH_4 is four-coordinate, S in SF_6 six-coordinate. However, in a 1-, 2-, or 3D structure one has more than one distance from a given atom to its neighbors, of course. One can plot a histogram of distances from symmetry-distinct atoms in a structure, shown in Figure 4a for a hypothetical square lattice of Sn atoms and Figure 4b for the real β-tin structure.

Such histograms, most of the time, have substantial gaps after the nearest neighbor contact, providing one possible definition of CN; but things are never simple. So in a 2D square lattice, one, of course, has a gap between a and $\sqrt{2}a$ (a is the atom–atom separation), as shown in Figure 4a (the first two bars, respectively). Notice, however, a larger gap to the next distance, $2a$. Should we call an atom in a square-planar lattice four- or eight-coordinate? It would be pretty silly to call it eight-coordinate, but which spatial gap in the histogram is larger?

In the β-tin structure, **4** (the bold-face numbers, here and subsequently, refer to the structure numbers in Figures 1–3), one has a flattened tetrahedron around a given Sn atom, with Sn–Sn 3.00 Å. Close to that is the separation of the reference atom from two further Sn atoms at 3.13 Å (shown in Figure 4b, the first two bars). It would be a mistake to call Sn, in the β-tin structure, four-coordinate, it really is closer to six-coordinate; CN = 4 + 2 might be a fairer description.

Sometimes the effective CN may be a function of the element chosen, given one and the same structural type. Consider the graphite polytype in Figure 1 (**1**), a simple hexagonal -AAAA- stacking of honeycomb layers. As we mentioned above, an atom in this structure could be called 3 + 2 coordinate, in which the additional two contacts are perpen-

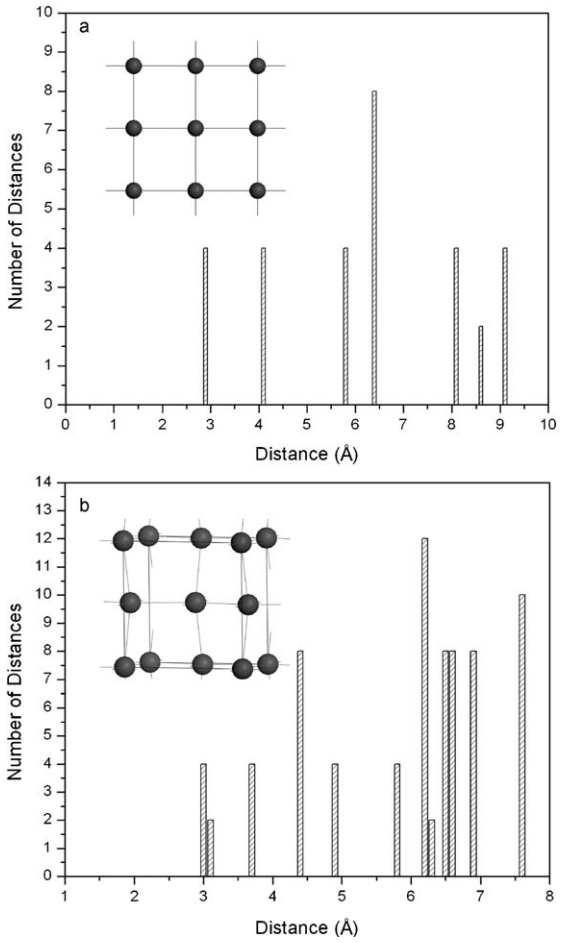

Figure 4. a) Histogram of distances from an atom in the 2D Sn square lattice (for Sn nearest neighbor separation of 2.881 Å); b) Histogram of distances from an atom in the 3D β-Sn lattice.

dicular to the honeycomb. For carbon the computed (not far from experimental) vertical contacts are 3.40 Å, the ones in the honeycomb net 1.42 Å. It makes sense to call each C in 3D graphite three-coordinate, rather than 3+2; even the next contact within the plane (≈2.5 Å) is shorter than the *c*-direction separation. But there might be instances for which the vertical contacts in this graphitic-type structure shorten, and/or the horizontal ones lengthen. For instance, this is the case for Pb, for which the computed distances in the above-cited graphite polytype structure (not that it's particularly stable) are 3.04 Å horizontal and 3.12 Å vertical. Here, 3+2 or five-coordination for Pb makes sense.

In addition there might be intermediate cases in which it is just best to throw up one's hands, and show a histogram of distances. Actually, Santiago Alvarez and co-workers have developed a very useful system of continuous shape and symmetry measures[4] (taking off from ideas of Avnir[5]) for studying just such cases of intermediate coordination.

Some background chemistry: The chemistry of C, Si, Ge, Sn, and Pb would take volumes to abstract, but perhaps it is worthwhile to summarize some obvious trends, as far as coordination number is concerned.

Carbon, of course, wants to be four, three, or two-coordinate. It is π-bonding that allows kinetically persistent low coordination in organic molecules. That π-bonding, for various reasons, does not play a stabilizing role in the chemistry of silicon and lower Group 14 congeners.[6] This is a point to which we will return below. Si occurs primarily in compounds with coordination number four, but excursions to coordination number five or six, and even (rarely) eight are very well known in discrete Si-containing molecules.

Around Sn one crosses the metal–nonmetal borderline at 1 atm. The structure of β-Sn shows six-coordination, and many discrete molecules of Sn are six-coordinate. At Pb one has a typical 12-coordinate metallic structure. However, discrete molecules contain Pb in a variety of coordination environments, from four up.

Later in this paper we will remark on a not unrelated matter, the average coordination number as derived from the radial distribution function of the liquid forms of these elements.

Results and Discussion

Overall energetics: The calculated energies of 29 structures for C, Si, Ge, Sn, and Pb are shown in Figures 5 and 6. Figure 5 plots the absolute formation energy, $\Delta E_f = (E_{tot} - N \times E_{atom})/N$ in which N = number of atoms in the unit cell, of each structure, per atom; Figure 6 plots the relative formation energy, per atom, relative to the most stable computed structure. Both display modes shown have their advantage.

It will be noted that some structures lack an entry. What this means is that the optimization beginning in that structural type led to a different geometry. In selected cases we will note when that happens. It may also be that a given entry (especially those of very high energy relative to other geometries), may not be a local minimum, but simply that the optimization has kept it in a specific space group.

Carbon: Clearly, carbon (open circles in Figures 5 and 6) has the most variation in energy between structures featuring different coordination, with a strong preference for three- or four-coordination (graphite and diamond). The 3D graphite and diamond formation energies are very low (by more than 2 eV per carbon) compared with the other carbon 3D lattices. When carbon is optimized starting with a β-Sn lattice, **4**, it rearranges into the diamond structure, **3**; thus there is no entry for structure **4** in Figures 5 and 6. The computed diamond structure is more favorable than both graphites (-ABAB- stacked structure, **1** and -AAAA-, **2**) by 0.02 eV. [Using the PAW-PBE functional (details in the Supporting Information), computed graphite is lower in energy than diamond, but the optimized graphite geometry was unrealistic—there is a big discrepancy from experiment in the *c* lattice parameter. The C–C computed bond lengths using both methods are reasonable.] Plane-wave-based DFT programs tend to have problems calculating correct dispersion

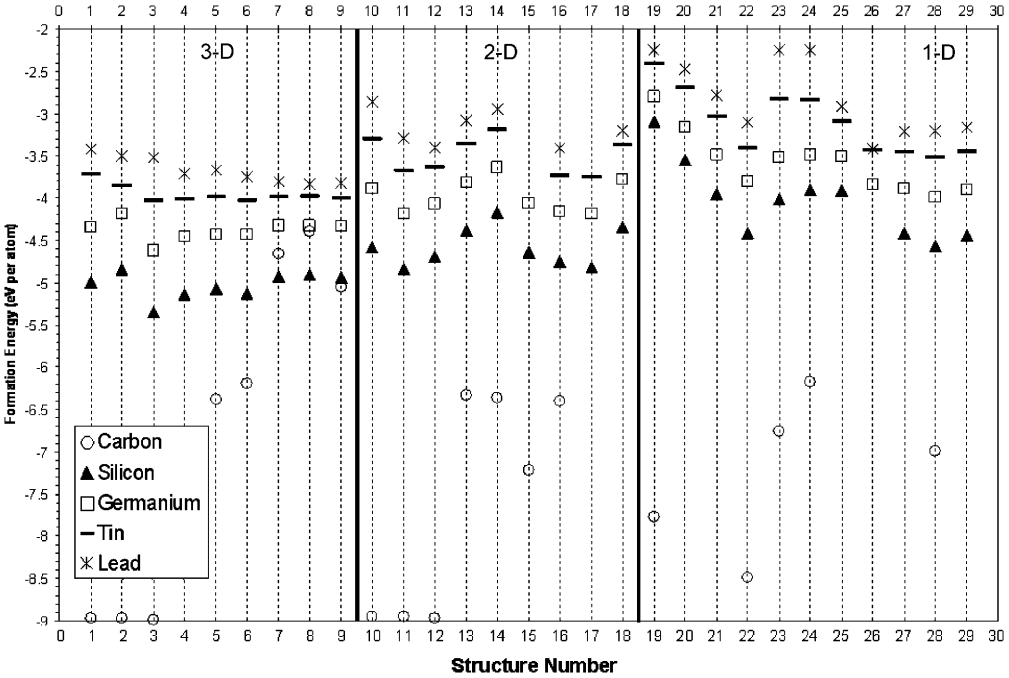

Figure 5. The formation energy per atom (see text) for C, Si, Ge, Sn and Pb in the 29 different starting geometries shown in Figures 1–3 (structure numbers refer to these figures). Note that there is no entry for some geometries; these rearrange to another more stable structure.

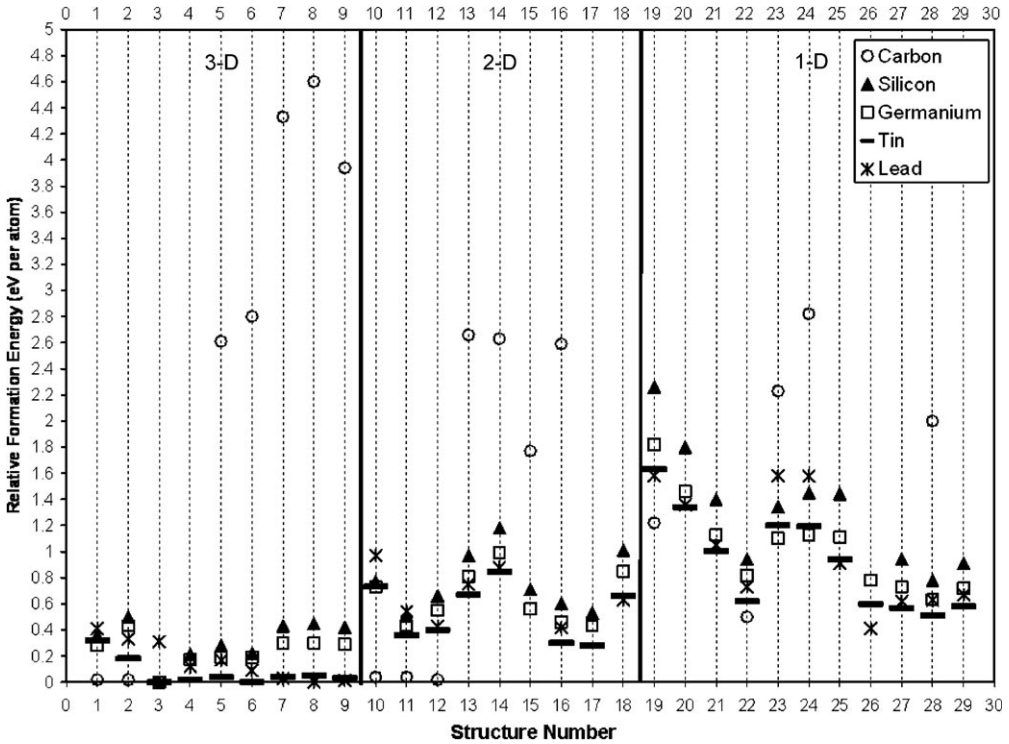

Figure 6. The relative formation energies (eV per atom) for C, Si, Ge, Sn, and Pb in the 29 different starting geometries shown in Figures 1–3. The reference point is the most stable computed structure, which is **3**, the diamond structure for C (see text), also for Si, Ge, and Sn. For Pb, the most stable computed structure is fcc, **8**.

energies; this is most likely the reason for this small discrepancy with experiment. The phonon dispersion calculation of graphite shows clearly two low frequency branches corresponding to C–C interactions between layers and also to a sliding of the layers (see the Supporting Information).

Carbon seeks out a lower coordination in 2D as well. The 2D graphene structure, **10**, with CN = 3 is low energy (0.04 eV less favorable than graphite). Zero-point energies are not included in our energies. We do not want to make much of this energy in view of our mistrust of dispersion force calculations with the DFT functional used. A graphene layer is in reality a little less stable than the same layer in graphite. The experimental range for the exfoliation energy of graphite extends from 35 to nearly 60 meV per atom.[7] The theoretical calculations (semiempirical and ab initio) for the exfoliation energy of graphite are even more variable; ranging from almost zero to more than 170 meV per atom.[8]

Carbon nanotubes[9] have garnered much attention over the last 20 years. So has a more difficult to characterize 1D structure, carbyne (a polyacetylenic valence structure, sometimes called *karbin*).[10,11,12] It is not surprising that the 1D linear chain (carbyne), **19** CN = 2, and the (3,3) single-walled nanotube (SWNT), **22** CN = 3, are the lowest energy 1D carbon species. We did not study other nanotubes. Were we to do so, it is likely that as we increase the diameter of the nanotube, the ring strain would diminish and the formation energy would approach graphene. Still, these 1D structures are less stable than graphene (2D) and graphite/diamond (3D). Notice the CN trend through dimensions—1D CN = 3, 2D CN = 3, and 3D CN = 3 or 4 are the preferred structures.

Other carbon structures occur at very high energy. There are glimpses of chemical relevance here and there. Consider the two simple 1D hypothetical carbon structures, **23** and **24**. Both are extended spirocycles (CN = 3 and 4), but **23** contains a tetrahedral carbon, **24** a square-planar carbon. A simple 90° twist results in a 0.5 eV per C energy stabilization favoring the linear polymer with tetrahedral carbon, **23**. This is hardly surprising given what we know of carbon chemistry, and the absence of special factors stabilizing square-planar carbon (a geometry close to the heart of one of us[13,14]).

Carbon is the only one of the Group 14 elements known to have metastable, kinetically persistent 1D (carbyne, nanotubes) and 2D (graphene) allotropes (and 0D, as well, counting the fullerenes). That fact is a consequence of barriers to oligo- and polymerization (for instance, carbyne to graphene) and bond reorganization. Our computed barrier to transformation from hexagonal diamond to graphite is $\approx$0.5 eV per carbon (11.6 kcal mol^{-1} per carbon), a subject to which we will return. This situation changes dramatically as we move down Group 14.

Silicon: The immediate and striking feature of the energies in Figure 5 is that all of the 3D Si structures (black triangles) computed are within 0.5 eV per Si of each other. Quite a difference from carbon! The fall from grace of the graphitic structures for Si (one of them is the least stable of the nine 3D structures) is not surprising. For carbon, the stability of graphite arises from partial multiple or π-bonding, a degree of aromatic stabilization. We know that after the second period multiple bonding is worth much less energetically.[6,15,16] For instance, there are many known unsaturated carbon compounds with π-bonding, with double, triple, and benzenoid bonds. However, this type of bonding is rare for Si. Chemists have to work very hard to make π-bonded silicon compounds; these are stable only when one engineers (using substituents) steric barriers to prevent reactivity.[17,18] All this is consistent with the relatively high energy of a graphitic silicon structure.

Diamond-type Si, four-coordinate, has the lowest computed formation energy (−5.35 eV per Si); experimentally this is the global minimum as well. Our computed diamond structure Si–Si distance is 2.34 Å (experimental 2.35 Å). Only 0.2 eV above the diamond structure are β-tin (**4**) and simple hexagonal (**6**) alternatives. The β-tin structure (**4**), as mentioned earlier, should be considered 4+2- or six-coordinate; the sh-type (**6**) six- or eight-coordinate (more below on this structure). The β-Sn-type Si has two kinds of Si–Si bonds (four at 2.47 Å in a flattened tetrahedron, two axial at 2.60 Å). Clearly, this structure is closer to six- than four-coordinate.

We wondered how big the barrier would be for the rearrangement of these metastable phases of Si to diamond (or vice versa). For Si (and Ge), this transformation from diamond-type (CN 4) to the metallic, tetragonal β-Sn-type structure (CN 6) can be effected experimentally by subjecting them to pressures of 200 (Si) and 120 kbar (Ge) along the *c* axis.[19] The transition from diamond-type α→β-Sn-type structures involves a deformation preserving the *c* axis, as shown in Figure 7 for two unit cells. Note the proportions of the unit cell change dramatically. The barrier to transformation from the α to β-Sn-type structure we compute for Si is small, only 0.1 eV per Si.

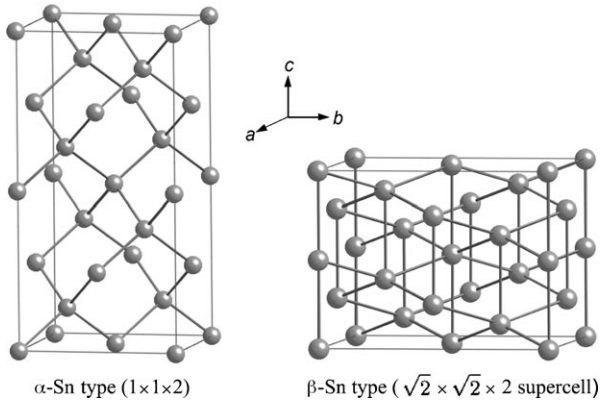

Figure 7. A path for transforming an α-Sn structure into the β-Sn structure through dilation in the *ab* plane, and concomitant compression along the *c* axis. In this way, the β-Sn-type ($\sqrt{2}\times\sqrt{2}\times 2$) supercell can be obtained.

The relatively low energy of the β-Sn structure for elemental Si is not surprising, given that there are six-coordinate molecular compounds of Si, but the relatively low

energy of the simple hexagonal structure deserves some comment. When optimized, simple hexagonal Si has two types of Si bonds (six in plane at 2.62 Å, two axial at 2.45 Å). Both distances are longer than a typical Si–Si single bond (2.35 Å), which would be expected. Interestingly, the two axial bonds are shorter, but the axial–equatorial bond length differential is too small for this structure to be called anything but eight-coordinate.

The trend in energy for 2D Si geometries is different from carbon. First, all the structures are within 1 eV of each other. Second, they are on average higher in energy than the 3D Si structures. We find that two-layer "graphitic" silicon, **11** (the reason for the quotes will be given below), is the favored 2D structure (with structure **17** right behind it). This is not surprising given that Si prefers to be four-coordinate—the two-layer "graphitic" structure **11**, not **12** provides this coordination, albeit not with ideal angles. The reasons for Si disfavoring three-coordination will be discussed in detail in the next section. In structure **11**, (Figure 8 top)

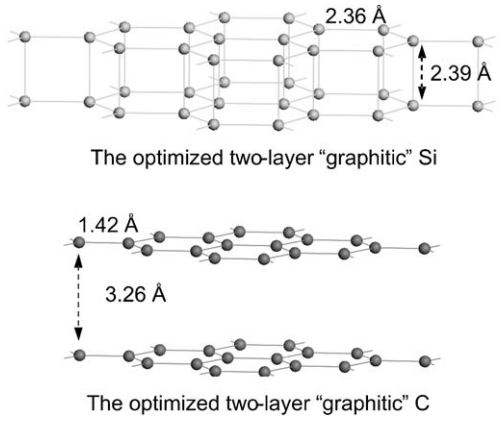

Figure 8. The optimized two-layer "graphitic" Si and C, starting with structure **11**.

there are three Si–Si bonds at 2.36 Å and one, vertical, at 2.39 Å. The local geometry (C_{3v}) is that of a distorted tetrahedron with some Si-Si-Si angles of 90°. The vertical distance in the two-layer C is 3.26 Å (Figure 8 bottom), which is similar to the layer distance in real graphite (3.35 Å).

The distortion at Si in structure **11** is somewhat analogous to that found at Si in the extended structure of $CaAl_2Si_2$.[20] A molecular model—truncating the element lattice and "passivating" the dangling valences with hydrogens—can provide insight into the cost of such a distortion: Figure 9 shows the energy of $E(EH_3)_4$ (E = C, Si, Ge, Sn, or Pb) for a deformation maintaining C_{3v} symmetry. The only variable in this potential energy surface is the angle. Clearly, Group 14 elements in symmetrical molecular models such as the ones chosen here prefer a perfect tetrahedron (T_d) to a distorted one (C_{3v}). The energetic cost of this transformation (measured, for instance by the difference in energy for $\alpha = 109.5 \rightarrow \alpha = 90°$) generally decreases down Group 14: C (2.5 eV) > Si ≈ Ge (0.9 eV) > Sn (0.5 eV) > Pb (0.3 eV).

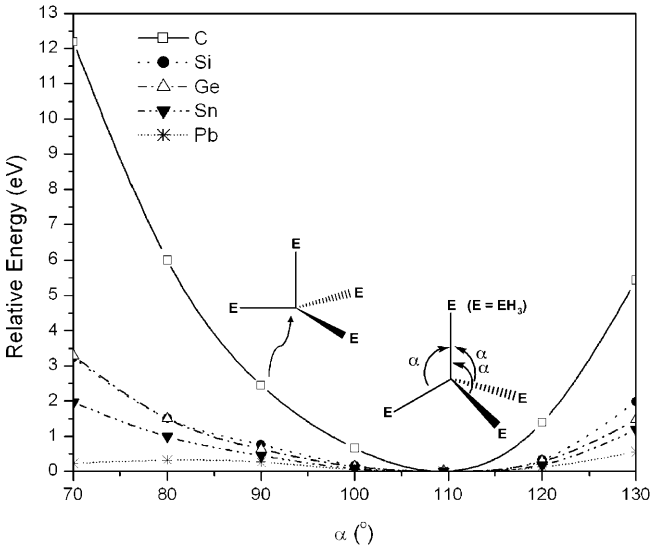

Figure 9. The potential energy surface of the transformation from a perfect tetrahedron T_d to a distorted C_{3v} tetrahedron for $E(EH_3)_4$, where E = C, Si, Ge, Sn, or Pb.

Structure **11** is thus a compromise. If the two graphene-like sheets of Si were separated by an infinite (hypothetical) distance, they would be ≈0.8 eV per Si above the α-Si structure (estimated from the energy of formation of a single graphene-like sheet of structure **10**, computed as −4.55 eV per Si). In **11**, the two graphene sheets collapse, forming an extra bond between sheets; for Si much is gained from four-coordination. The strain resulting (0.9 eV per Si from the molecular model) is worth it.

Note the great difference between C and Si for the two-layer graphitic structures. For C, no bonds are formed between layers, only dispersion forces hold them together. For Si, the system forms as many single bonds as it can vertically. The next section explores this phenomenon down the group.

Structure **12**, the other graphitic polytype, has two different kinds of Si atoms—a three-coordinate Si with three axial Si–Si bonds at 2.36 Å and a four-coordinate Si with three axial Si–Si bonds at 2.36 Å and one vertical Si–Si at 2.40 Å. As expected, it is at higher energy than **11**; collapse of the two layers makes only half the atoms four-coordinate.

The square-planar and kagome nets (**13**, **14**) are high energy for Si; they are far away from the preferred tetrahedron even though they are four-coordinate. In a molecular $Si(SiH_3)_4$ model it costs 4.5 eV (see the Supporting Information) to go from tetrahedral to square-planar. The disfavoring of planar four-coordinate structures is greater for C than for Si; this shows up in molecular models as well. Two other 2D structures of relatively low energy are **16** and **17**; in these, Si is five- and six-coordinate, respectively. While distorted, these feature a coordination number that is not untypical for Si.

Monolayer graphene-type Si (**10**) is substantially higher in energy per Si than two-layer **11**, a great contrast to the carbon case, There is some π-bonding in **10**—notice the Si–

Si bond length of 2.23 Å compared to 2.35 Å in diamond-type Si, a shortening comparable to what happens for C. However, while structure **11** for C consists of essentially two graphene sheets bound by weak dispersion forces, **11** for Si, as we saw, collapses to a strained four-coordinate Si structure. Though π-bonded, a graphene-like Si sheet would much rather gain a fourth bond, even if the price of strain energy must be paid.

The 1D Si structures are even less stable than the 2D ones. The lowest energy one—the hexagonal pipe **28**—as well as **27** and **29** nearby in energy, are all four-coordinate. Clearly, that coordination is sought, even at the cost of unusual distortion. No doubt one-dimensional pieces of the diamond structure, even if they contain lower coordination terminations on the outside, could compete with these strained chains.

Given the current interest in graphenes, we turn next to a detailed analysis of single and multilayer graphene-like structures for all the Group 14 elements.

Graphene and graphitic structures in Group 14: The ability to make and study multi- and monolayer graphene structures has engendered much theoretical work.[21,22] A chemical perspective on what one would expect as one moves down Group 14 is useful as one looks at much speculation in the literature.

In Figure 10, we show the basic structures of interest, already included in our study, but useful to group together here. Structure **1** is the -ABAB- 3D graphite structure, structure **2** a simple hexagonal polytype, -AAAA- stacking, **10** is the 2D single layer graphene, **11** a two-layer -AA- stacked graphene, and **12**, a two-layer -AB- stacked graphene. Figure 10 shows the formation energies of these 3D and 2D geometries from the atoms.

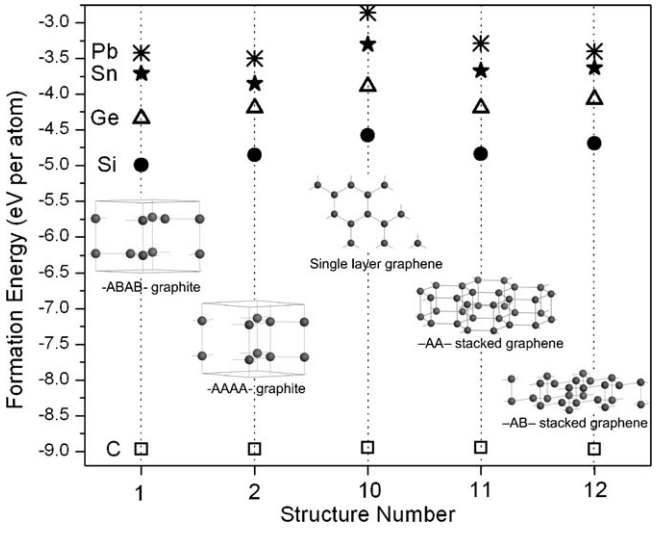

Figure 10. The energetic and schematic structural landscapes of Group 14 graphite (-ABAB- and -AAAA-), graphene-type (single layer, -AA- and -AB- two layer stacked) structures.

The essential piece of chemical intuition that is needed to make sense of the energetics is that π-bonding in Group 14, ideal in all the graphene structures, is a good thing only for carbon, and *not* for Si, Ge, Sn, and Pb. For these last elements, four-coordinate structures (of which diamond is archetypical) are favored. The reasons for this remain under discussion;[15,16] we think they are to be found in the poor π-type overlap between neighboring *n*p orbitals at the distance imposed by normal σ bonding. To be specific, the π overlap for the 2p orbitals of C at 1.42 Å is much bigger than for the 3p orbitals of Si at 2.34 Å. The result of this is shown in the schematic orbital interaction diagram (Scheme 1). Greater

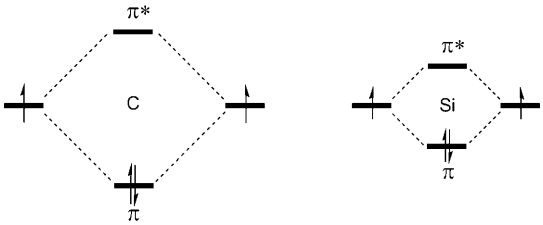

Scheme 1. A schematic of the π-type overlaps for C and Si planar systems.

overlap leads to more stabilization (a thermodynamic criterion). The same reduced π overlap in Si=Si double bonds leads to higher reactivity as well; the low-lying π*, the high-lying π orbitals are likely to make Si=Si highly reactive to bases and acids.

This rough notion (for an elaboration, see references [15,16]) is supported by the energetics, already mentioned, of diamond, **3** versus graphites **1** and **2**: similar in energy for C, quite different in energy for Si, Ge, Sn, and Pb.

The stability of C graphene layers, contrasted with the instability of corresponding Si, Ge, Sn, and Pb layers, lead to very different behavior of such layers on aggregation. The first piece of evidence for this is in the calculated equilibrium structures of the graphites **1** and **2**. The computed E–E inter- and intralayer distances in **1** are listed in Table 1. Note the gigantic difference between an intralayer bond (1.42 Å) and a van der Waals separation (3.32 Å) for C, while all the other Group 14 graphites have equalized intra- and interlayer distances. They have essentially collapsed to 3+2 or five-coordinate structures with bonds between layers.

Table 1. The E–E distances in -ABAB- graphite-type structure.

	Intralayer E–E distance [Å]	Interlayer E–E distance [Å]
C	1.42	3.32
Si	2.34	2.48
Ge	2.51	2.61
Sn	2.88	2.93
Pb	3.03	3.01

The collapse is likely activation-less. We simulated the process of bringing together 2D graphene-type (**10**) layers together as shown in Figure 11. Note the weak (dispersion

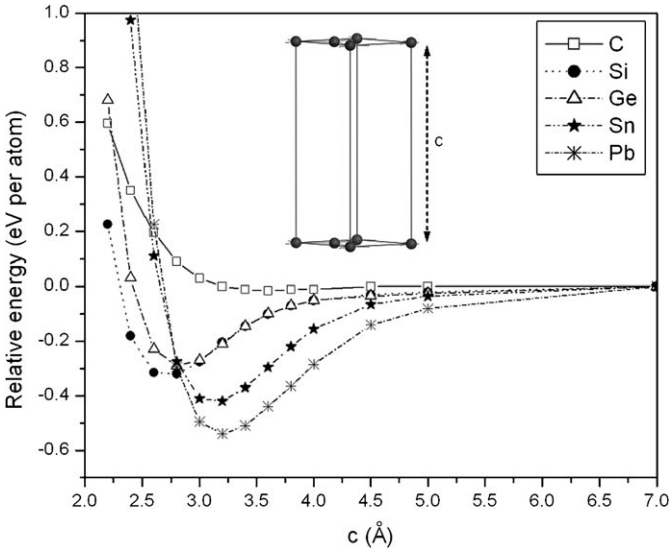

Figure 11. The relative energy (relative to the corresponding infinitely separated structure) of bringing 2D graphene-type sheets (**10**) together to form the -AAAA- graphite polytype.

force driven) aggregation of the C layers, and the pronounced activation-less bond-forming aggregation of the Si, Ge, Sn, Pb structures. To put it as directly as possible—graphene-like sheets of Si, Ge, Sn, and Pb are most unlikely to have an independent existence. If they are to be found, they will have to be intercalated by other atoms or molecules, or otherwise protected from reacting with each other. Such multilayer Si, Ge, Sn, and Pb graphenes, if made, will, of course, be interesting, just because they will self-condense to a 3D structure or to multilayer approximations thereto.

We also looked at the band structures of the various graphenes. The graphene-type Si structure is semimetallic, similar to C graphene. The Ge, Sn, and Pb structures, however, are metallic, with a σ* band crossing the Fermi level. The corresponding band structures are shown in the Supporting Information.

Germanium: Elemental germanium crystallizes in the diamond-type lattice at 1 atm and this is also computed to be its lowest energy structure. Ge is a metalloid with a similar electrical resistivity to Si at room temperature, but with a much smaller band gap. Its melting and boiling points and bond energy[19] (shown in Table 2) are also smaller than for Si, and this trend continues for Sn and Pb, which are both soft, low-melting-point metals. At pressures above 12 GPa, Ge crystallizes in a β-Sn-type structure. This transformation leads to a change in coordination from four to six. Diamond-type Ge has four equal Ge–Ge bonds at 2.45 Å; β-tin-type Ge has two kinds of Ge–Ge bonds (four at 2.64 Å in a

Table 2. The melting points, boiling points, and E–E bond energies of Group 14 elements.

	C	Si	Ge	Sn	Pb
melting points [K]	4373	1693	1218	505	600
boiling points [K]	–	≈3553	3123	2896	2024
E–E bond energies [eV]	3.69	2.35	1.95	1.57	1.02

flattened tetrahedron, two at 2.79 Å). Note the difference in axial/equatorial distance ratio from Si; in Si the axial bonds are shorter. We computed the potential barrier for the transformation from diamond to β-tin-type Ge (shown in the Supporting Information) to be only 0.15 eV per Ge.

In its computed structural preferences, germanium emerges as remarkably similar to silicon. Note how closely the energies of various Ge structures follow their Si analogues. The diamond lattice is the most stable; almost all of the 3D structures are more stable than the 2D ones, and the most stable 2D structures are more stable than all of the 1D structures considered. Ge clearly prefers to be four-coordinate, as does Si. However, five-, six-, and higher CN structures are not penalized much energetically.

Tin: Tin, along with carbon, is the most interesting of the Group 14 elements. It has long been known that two stable Sn allotropes—grey tin or diamond-type (**3**, α-Sn) and white tin (**4**, β-Sn) are found at ambient temperature and pressure. The transformation between the two phases takes place at 12 °C at $P=1$ atm. Grey or α- tin is four-coordinate with four Sn–Sn bonds at 2.81 Å; white or β- tin is six-coordinate and has two kinds of Sn–Sn bonds (four at 3.00 Å in a flattened tetrahedron, two at 3.13 Å). A structural distortion along the *c* direction of the β-Sn lattice leads to the diamond-type and vice versa. We computed the energy barrier between α and β tin as 0.20 eV per Sn for transformation by this mechanism. α-Sn is computed as 0.04 eV per Sn more stable than the β-isomer.

The computed energetics shown in Figures 5 and 6 suggests that a number of different tin allotropes may be competitive in energy. If we use α-tin (**3**) as the reference structure, structures **4**–**9** are within 0.02 eV of α-Sn. Clearly, graphitic Sn structure (**1** and **2**) are the highest energy species and also have the lowest coordination (CN = 3 + 2 or 3 and 5), but even they are < 0.05 eV/Sn above α-Sn. The very highly coordinated structures (CN 12), **8** (fcc, Sn–Sn 3.32 Å) and **9** (hcp, Sn–Sn 3.32 Å), are also competitive with α- and β-Sn.

The strong discrimination against π-bonded three-coordinate structures we noted for Si continues for Sn, So **10**, a single graphene-like sheet, is less stable than the collapsed, strained four-coordinate **11**. All 2D and 1D structures are less stable than the 3D ones.

Let's return to the essential finding for Sn; aside from a real dislike for a CN = 3, all 3D structures have nearly the same energy. We are investigating the barriers between the various structures; the preliminary conclusion is that they are small. The conclusion is not surprising; Sn is a low-melt-

ing solid, with a melting point of 505 K. Having all ordered structures close to each other in energy is a hint that one is dealing with a material close to a liquid. We will return to this perspective.

Lead: Let us now come back to the starting point for our study, Pb structures. Pb clearly prefers high coordination. The difference in energy between fcc (**8**, the most stable structure) and graphite (**1** and **2**) is only 0.40 eV; the rest of the 3D structures are found in between the two energetic extremes. We plotted the potential energy surface (see the Supporting Information) for the transformation from bcc (**7**) to fcc (**8**); note that an fcc structure is identical to a bct structure with $c/a=\sqrt{2}$. The energy of activation for this Bain transformation is zero.[23,24] The twelve Pb–Pb near neighbor separations in fcc Pb are computed as 3.45 Å, while the eight Pb–Pb bond lengths in the bcc structure are 3.35 Å.

By way of an oversight in our 2D computations, we came across an interesting trend for Pb. Optimizations of Pb in the structure **15** (corrugated square sheet) geometry led to a structure like **17** (trigonal prism sheet), but not identical to that shown in Figure 2. Instead, the bridging atoms migrated to fourfold sites; the result is an eight-, not a six-coordinate species. Subsequent optimizations of this eight-coordinate Pb variant of **17** led us back to the fcc structure.

Liquids and the problems of defining first coordination numbers in them: What we saw in our calculations of ordered crystalline structures as we go from C to Pb is pretty simple:

1) The preferred structures move from low (3, 4) coordination number to high (12).
2) The energies of all the possible structures come closer together, especially for Sn and Pb.

Clearly the latter observation is consistent with approach to a liquid. The relatively low melting points of Sn (505 K) and Pb (600 K) agree. The coordination number preferences are likely to extend to the liquid state. Let us then approach a description of the liquid state of these elements.

Given relative local order and long-range disorder, distance correlation functions are essential tools in the description of liquids. The literature defines a variety of correlation and distribution functions; let's try for a clear definition. The pair distribution function $g(r)$ is defined as the probability of finding another atom a distance r from the reference atom, relative to the random average probability; $g(r)\rightarrow 1$ as $r\rightarrow\infty$, and $g(r)\rightarrow 0$ at $r=0$. A typical $g(r)$ for liquid Pb (from our calculations) is sketched in Figure 12.

A radial distribution function (RDF) is $4\pi r^2\rho g(r)$, in which ρ is the average number density, N/V, $N=$number of particles, $V=$volume. This is the number of atoms or molecules in a spherical shell around r. The value of $g(r)$ can be computed or can be extracted (with some work) from X-ray or neutron diffraction experiments.[25]

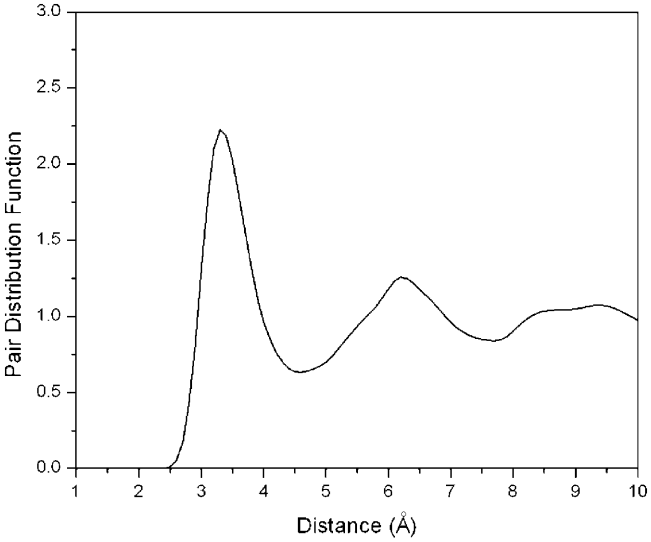

Figure 12. Pair distribution function of liquid Pb at 1500 K.

It is clear that the number of nearest neighbors in a liquid, to the extent that it can be defined, is related to the area under the first peak in $4\pi r^2\rho g(r)$. To get more quantitative, and estimate an effective first coordination number in a liquid, has not been easy. At least four methods to compute the coordination number from the radial distribution function may be found in the literature:[26,27] These are: A) a "completion" of the first peak using the function rg(r) about a radius of symmetry; B) a similar symmetrization using the function $4\pi r^2\rho g(r)$ about its first maximum; C) a decomposition of the function $4\pi r^2\rho g(r)$ into first, second, and so forth, shells; and D) integrating the function $4\pi r^2\rho g(r)$ to the first minimum in the radial distribution function. The four methods are shown schematically in Figure 13.

Mikolaj and Pings[27] give a detailed comparative analysis of these four methods for computing the coordination number. These is much variation: for liquid argon, they obtained CN of 5.3 by method (A), 6.0 by (B), 6.6 by (C), and 7.5 by (D). What is worse, people are not very conscientious in specifying which method they use.

For the elements of interest to us, the absolute numbers are (to give a generous characterization) ambiguous. Cahoon[28] calculated first coordination numbers for liquid Si, Ge, Sn, and Pb as 4.7, 5.0, 6.7 and 7.3, respectively. Tao[29] predicted the coordination numbers for liquid Si, Ge, Sn, and Pb as 7.9, 7.8, 9.2 and 10.5. Swalin,[30] in his fluctuation theory of diffusion, used a value of ten for the first coordination number for Sn, while Hines et al.[31] suggest a value of six for Sn, based on the relationship between the empty volume fraction and the number of nearest neighbors in solid metals to the liquid state. In Group 14, even as everyone agrees that the coordination numbers rise from liquid Si to Pb, there clearly is substantive disagreement on the CN values.

In a recent study, Ganesh and Widom[32] provided good computational evidence for a liquid-to-liquid phase transi-

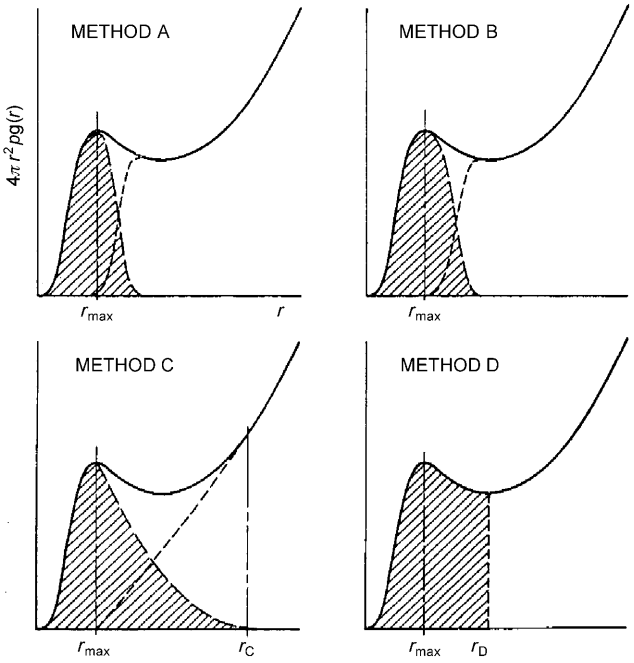

Figure 13. The four methods for computing the coordination number (from reference [27])

tion in silicon. They find a low-density low-coordinate (CN = 4.2 at 1182 K by method D) semimetallic liquid coexisting with a high-density metallic liquid with higher CN (5.6).

Simulating Group 14 liquid structures: Our own primitive approach to the liquid state of Si, Ge, Sn, and Pb uses a high-temperature molecular dynamics calculation. MD calculations were performed for Si, Ge, Sn, and Pb at 3000, 2000, 1500, and 1500 K, respectively; the temperatures were chosen to ensure that the elements were in the liquid state. The starting structures (over 200 atoms in supercell) were ordered diamond Si and Ge, β-Sn, and fcc-Pb. Next, we evaluated the radial distribution function, $g(r)$ from the liquid configurations obtained by MD calculation (details in the Supporting Information). The parameters obtained, including the temperature (T in K) of the MD calculation, RDF curve information (r_0 and r_{min} in Å), the corresponding atomic density ($\rho = N/V$ in Å^{-3}) and calculated coordination number (CN_{calcd}) are shown in Table 3.

First coordination numbers were calculated by integrating the radial distribution function $4\pi r^2 \rho g(r)$ to the first minimum for liquid Si, Ge, Sn, and Pb (method D of Figure 13). The values obtained are 5.1, 7.1, 8.7, and 10.4, respectively. As might have been anticipated from the review of the literature above, the trend is as expected, but these values are not exactly in agreement with other studies. From experiment,[33] the coordination numbers of Si, Ge, Sn, and Pb are 6.4, 6.8, 10.9, and 10.9, respectively. The calculated percentage deviation from the experimental values is 20.3% (Si), 4.4% (Ge), 20.2% (Sn), and 4.6% (Pb). Such an outcome falls within the expected range of deviation for many liquid

Table 3. Computed parameters from the simulation of liquid states of Si, Ge, Sn, and Pb: liquid temperature (T) in molecular dynamics calculations, approximate r_0 and r_{min} position from the RDF curve, corresponding atomic density ($\rho = N/V$), and calculated coordination number (CN_{calcd}) and experimental coordination number (CN_{exptl}), and deviation.

	T [K]	r_0 [Å]	r_{min} [Å]	ρ [Å^{-3}]	CN_{calcd}	CN_{exptl}[33]	Deviation [%][a]
Si	3000	1.70	3.50	0.0507	5.1	6.4	20.3
Ge	2000	1.90	4.00	0.0444	7.1	6.8	4.4
Sn	1500	2.20	4.20	0.0382	8.7	10.9	20.2
Pb	1500	2.50	4.50	0.0345	10.4	10.9	4.6

[a] Percentage deviation $= [(CN_{calcd} - CN_{exptl})/CN_{exptl}] \times 100$, in which CN_{calcd} and CN_{exptl} are the calculated and experimental values, respectively.

metals.[34] In the work of Hines et al.,[34] coordination numbers were predicted for 39 liquid metals, with average deviations of 13 or 23% from the literature values, depending on the method of calculation. Note that we studied liquid Si only at one temperature and pressure; thus there is no way we could pick up the fine points of the liquid Si structure found by Ganesh and Widom.[25]

Concluding Comments

As expected, coordination number is a determining factor in the crystalline (and liquid phase) structures of Group 14 elements, and the preferred coordination of extended structures is closely related to the bonding preferences (call them loosely the valence of the atom) of discrete molecules containing the atom.

So carbon not only favors four-coordination, but also is quite happy with π-bonding, allowing three- and even two-coordination to compete. Highly coordinated ($CN > 4$) carbon molecules are rare, and that carries over to preferences in extended structures. For every other Group 14 element π-bonding is neither thermodynamically nor kinetically a good thing.

An immediate consequence of the above regularities, very much chemical in origin, is the destabilization of simple graphene sheets (relative to higher coordination structures), and the likely collapse of multigraphene layered arrays to four-coordinate structures.

Si and Ge are quite similar to each other, even as they are different from C. Higher coordination structures become competitive for these elements. Sn and Pb favor still higher coordination; for these last elements all higher coordination structures are roughly at equal energy. This, of course, is a harbinger of their low melting point. The Group 14 liquid structures we simulate in molecular dynamics calculations show the expected effective first coordination number increase down Group 14.

In a future paper we will explore how this structural landscape evolves as the pressure changes, and as we move to more ionic structures.

Computational Methods

In each case the structure was optimized in its own space group. The energies are given relative to the lowest energy spin state of each atom. The calculations are based on the plane wave/pseudopotential approach using the VASP (Vienna Ab-initio Simulation Package)[35–,3637] computer program, employing the local density approximation (LDA) and the projected-augmented wave (PAW)[38,39] formalism. The energy cutoff used for plane waves was 500 eV. A Monkhorst Pack grid of k-points was used. In order to model one-dimensional structures, as VASP is a three-dimensional computational method, we inserted a large vacuum layer (≈15 Å) in the **a** and **b** direction, while still allowing all unit cell parameters to vary. For the two-dimensional structures a vacuum layer was inserted in the **c** direction. For MD simulation, the only Γ k point were conducted at the energy cutoff of 400 eV. A 3 fs time step is utilized.

Acknowledgements

We are grateful to Neil W. Ashcroft, Benjamin Widom, and Michael Widom for discussions, and Santiago Alvarez for sending us an important paper prior to publication. Calculations were performed in part at the Cornell NanoScale Facility, a member of the National Nanotechnology Infrastructure Network, which is supported by the National Science Foundation. Our work at Cornell was supported by the National Science Foundation through Grant CHE-0613306 and CHE-0910623. This research was also supported by the National Science Foundation through TeraGrid resources provided by NCSA.

[1] C. N. R. Rao, A. K. Sood, K. S. Subrahmanyam, A. Govindaraj, *Angew. Chem.* **2009**, *121*, 7890–7916; *Angew. Chem. Int. Ed.* **2009**, *48*, 7752–7777.
[2] M. Eschen, W. Jeitschko, *J. Solid State Chem.* **2002**, *165*, 238–246.
[3] X.-D. Wen, T. J. Cahill, R. Hoffmann, *J. Am. Chem. Soc.* **2009**, *131*, 2199–2207.
[4] A. Ruiz-Martínez, D. David Casanova, S. Alvarez, unpublished results.
[5] S. Alvarez, P. Alemany, D. Casanova, J. Cirera, M. Llunell, D. Avnir, *Coord. Chem. Rev.* **2005**, *249*, 1693–1708.
[6] P. P. Power, *Chem. Rev.* **1999**, *99*, 3463–3504.
[7] a) L. A. Girifalco, R. A. Lad, *J. Chem. Phys.* **1956**, *25*, 693–697; b) L. X. Benedict, N. G. Chopra, M. L. Cohen, A. Zettl, S. G. Louie, V. H. Crespi, *Chem. Phys. Lett.* **1998**, *286*, 490–496; c) R. Zacharia, H. Ulbricht, T. Hertel, *Phys. Rev. B* **2004**, *69*, 155406.
[8] a) N. L. Allinger, *J. Am. Chem. Soc.* **1977**, *99*, 8127–8134; b) S. B. Trickey, F. Müller-Plathe, G. H. F. Diercksen, J. C. Boettger, *Phys. Rev. B* **1992**, *45*, 4460; c) H. Rydberg, N. Jacobson, P. Hyldgaard, S. I. Simak, B. I. Lundqvist, D. C. Langreth, *Surf. Sci.* **2003**, *532*, 606–610.
[9] S. Iijima, T. Ichihashi, *Nature* **1993**, *363*, 603–605.
[10] R. H. Baughman, *Science* **2006**, *312*, 1009–1010.
[11] *Carbyne and Carbynoid Structures* (Eds.: R. B. Heimann, S. E. Evsyukov, L. Kavan), Springer, Berlin, **1999**.
[12] *Polyynes: Synthesis Properties and Applications* (Ed.: F. Cataldo), Taylor & Francis, Boca Raton, **2005**.
[13] a) R. Hoffmann, R. W. Alder, Jr., C. F. Wilcox, *J. Am. Chem. Soc.* **1970**, *92*, 4992–4993; b) P. D. Pancharatna, M. A. Méndez-Rojas, G. Merino, A. Vela, R. Hoffmann, *J. Am. Chem. Soc.* **2004**, *126*, 15309–15315.
[14] R. Keese, *Chem. Rev.* **2006**, *106*, 4787–4808, and references therein.
[15] "Theory of Organosilicon Compounds": Y. Apeloig in *The Chemistry of Organosilicon Compounds* (Eds.: S. Patai, Z. Rappoport), Wiley, New York, **1989**, pp. 57–225.
[16] "Theoretical Aspects of Compounds Containing Si, Ge, Sn and Pb Compounds": M. Karni, Y. Apeloig, J. Kapp, P. von R. Schleyer in *The chemistry of Organic Silicon Compounds, Vol 3* (Eds.: Z. Rappoport, Y. Apeloig), Wiley, New York, **2001**, pp. 1–163.
[17] R. West, M. J. Fink, J. Michl, *Science* **1981**, *214*, 1343–1344.
[18] A. Sekiguchi, R. Kinjo, M. Ichinohe, *Science* **2004**, *305*, 1755–1757.
[19] N. N. Greenwood, A. Earnshaw, *Chemistry of the Elements*, 2nd ed., Butterworths/Heinemann, Oxford, **1997**, Chapter 10, p. 372.
[20] C. Zheng, R. Hoffmann, *J. Solid State Chem.* **1988**, *72*, 58–71.
[21] M. Klintenberg, S. Lebègue, C. Ortiz, B. Sanyal, J. Fransson, O. Eriksson, *J. Phys. Condens. Matter* **2009**, *21*, 335502.
[22] A. H. Castro Neto, F. Guinea, N. M. R. Peres, K. S. Novoselov, A. K. Geim, *Rev. Mod. Phys.* **2009**, *1*, 109–163.
[23] E. C. Bain, *Trans. AIME* **1924**, *70*, 25–35.
[24] S. Lee, R. Hoffmann, *J. Am. Chem. Soc.* **2002**, *124*, 4811–4832.
[25] Y. Marcus, *Introduction to Liquid State Chemistry*, Wiley, New York, **1977**.
[26] Y. Waseda, *The Structure of Non-crystalline Materials: Liquids and Amorphous Solids*, McGraw-Hill, New York. **1980**.
[27] P. G. Mikolaj, C. J. Pings, *Phys. Chem. Liq.* **1968**, *1*, 93–108.
[28] J. R. Cahoon, *Can. J. Phys.* **2004**, *82*, 291–301.
[29] D. P. Tao, *Metall. Mater. Trans. A* **2005**, *36*, 3495–3497.
[30] R. A. Swalin, *Acta Metall.* **1959**, *7*, 736–740.
[31] A. L. Hines, H. A. Walls, D. W. Arnold, *Metall. Trans. B* **1975**, *6*, 484.
[32] P. Ganesh, M. Widom, *Phys. Rev. Lett.* **2009**, *102*, 075701.
[33] Y. Waseda, in *Liquid Metals* (Eds.: R. Evans, D. A. Greenwood), **1976**, IOP, London, **1977**.
[34] A. L. Hines, H. A. Walls, K. R. Jethani, *Metall. Trans. A* **1985**, *16*, 267–274.
[35] J. P. Perdew, K. Burke, M. Ernzerhof, *Phys. Rev. Lett.* **1996**, *77*, 3865.
[36] G. Kresse, J. Hafner, *Phys. Rev. B* **1993**, *47*, 558.
[37] G. Kresse, J. Hafner, *Phys. Rev. B* **1994**, *49*, 14251.
[38] P. E. Blöchl, *Phys. Rev. B* **1994**, *50*, 17953–17979.
[39] G. Kresse, D. Joubert, *Phys. Rev. B* **1999**, *59*, 1758–1775.

Received: November 14, 2009
Published online: May 19, 2010

